SCAN-LINE QUALITY INSPECTION OF STRIP MATERIALS USING 1-D RADIAL BASIS FUNCTION NETWORK

Afşar Saranlı
Dept. of Electrical and Electronics Eng., Middle East Technical University,
İsmet İnönü Bulv.,06531 Ankara, Turkey

Keywords: Automated Optical Inspection, Radial-Basis Functions, Gaussian Mixture Models, Image Event Detection.

Abstract: There exist a variety of manufacturing quality inspection tasks where the inspection of a continuous strip of material using a scan-line camera is involved. Here the image is very short in one dimension but unlimited in the other dimension. In this study, a method of image event detection for this class of applications based on adaptive radial-basis function networks is presented. The architecture of the system and the adaptation methodology is presented in detail together with a detailed discussion on parameter selection. Promising detection results are illustrated for an application to grinded glass edge inspection problem.

1 INTRODUCTION

Automating the quality inspection process is an application field of computer vision which is increasingly becoming a major need for many industries (Malamas et al., 2003) . This is due to factors such as the increasing market pressure for concurrently lowering product costs and increasing product quality; the variation and subjectivity in the performance of human operators in the inspection process and the requirements on the speed-throughput of the process. Industries where this pressure is especially intense include, among others, the glass manufacturing for the automotive and CRT markets, the production of the TFT-LCD panels as well as the inspection of textiles. (Kim et al., 2001) (Cho et al., 2005)

Almost all of these applications require the real-time non-contact inspection of material flowing through the production line. A feasible way of achieving this is through automated optical inspection, often abbreviated as AOI, where a camera is used to detect production defects. If the material being inspected is moving or can be moved at controlled speed, the use of a scan-line camera or a TDI line-scan camera (if better illumination sensitivity is required) is appropriate.

Systems using a scan-line camera for inspection generates a continuous run of image data with one comparatively smaller image axis and a comparatively large other image axis. The digital processing of such strips of images often require either buffered algorithms along the scanning direction, or preferably, scan-line based algorithms since they are a better match for the data generation process.

2 PROBLEM DESCRIPTION

Image processing for the inspection of a material on the production conveyor consist of modelling the material's normal image behaviour as it flows through the conveyor. The task is then to perform a detection of the anomalous or defective behaviour on the material based on changes in the scan-line signal.

A class of problems is when the material is a smooth but scattering surface such as the side view of a manufactured pipe, top view of railway tracks (Alippi et.al., 2000) or the grinded edge of a glass sheet. Such a scan-line camera signal is illustrated in Figure 1.

Saranlı A. (2006).
SCAN-LINE QUALITY INSPECTION OF STRIP MATERIALS USING 1-D RADIAL BASIS FUNCTION NETWORK.
In *Proceedings of the First International Conference on Computer Vision Theory and Applications*, pages 19-26
DOI: 10.5220/0001366300190026

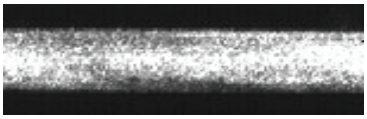

Figure 1: Scan-line image of material edge.

In this case, the normal signal profile has a reasonable degree of smoothness corrupted by noise due to the scattering properties of the surface or the nature of the illumination. For non-defective material, the signal behaviour does not change along the scanning direction. Defects on the other hand behave as unexpected and often fast changes in the signal behaviour along the scanning direction. When the cross-section (or the scan-line) of the inspection image is considered, The Radial Basis Function network with its smoothed approximation properties appears to be ideally suited to model the behaviour of the signal (Haykin 1999; Poggio and Girosi 1990). In fact, RBF networks have been successfully used in a number of detection applications (Ahmet W. et al., 1994; Leung H. et al., 2002; Shen M. et al., 2005).

Modelling the single scan-line with a 1-D RBF effectively addresses the problem of suppressing the noise while retaining the overall signal behaviour in each scan-line. The next important problem is the detection of the anomalous behaviour (or defects) based on the model of the scan-line and a sequence of the scan-line data from the image. We address this problem in the following section by introducing the RBF model of the scan-line a model mismatch based detection algorithm.

3 THE RBF MODEL AND MODEL MISMATCH DETECTION

3.1 The 1-D RBF Scan-line Model

The proposed scan-line model is given by

$$\hat{r}[n] = \sum_{i=1}^{M} p_i \exp\left[\frac{-(n-\mu_i)^2}{2\sigma_i^2}\right] \quad (1)$$

Based on the behaviour and the required smoothness of the scan-line signal, a model order is chosen. Figure 2 illustrates a model with M=7 and M=5 Gaussian basis functions superimposed with the actual noise corrupted scan-line signal. The edge region contains approximately 2 basis functions.

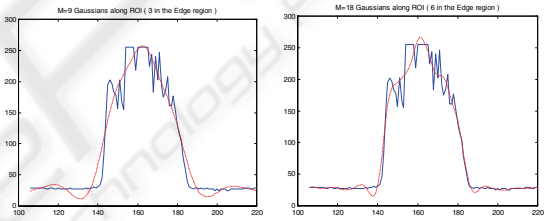

Figure 2: RBF Approximations to the scan-line signal.

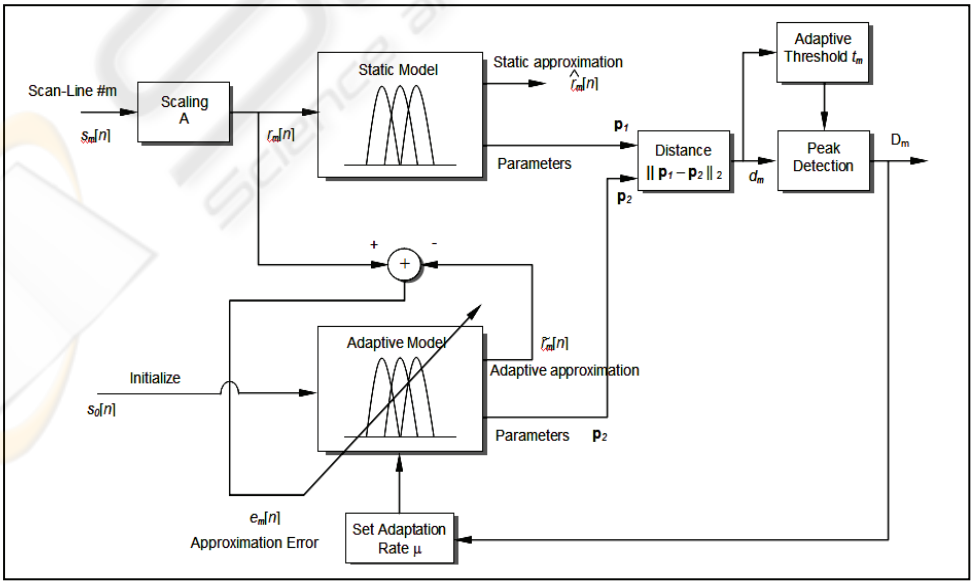

Figure 3: The block diagram of the model mismatch based defect detection algorithm.

3.2 Model Mismatch Based Detection Algorithm

The defect detection algorithm is based on the assumption that the normal edge behaviour is almost stationary (or with very slow variation) across subsequent scan-lines while an anomaly or defect is an unexpected (and comparatively fast) change in this behaviour. Therefore, we propose a detection algorithm based on the model mismatch between a direct *static* approximation to the current scan-line data and a slowly varying (tracking) *adaptive* approximation which performs a smoothing over the history of scan-line data. A block diagram of this model mismatch based detection algorithm is illustrated in Figure 3.

The proposed detection algorithm maps a sequence of scan-line image data $S_m[n]$ into a binary detection signal D_m. This is achieved by the following procedure: Each m[th] 1-D scan-line signal data is modelled my a 1-D approximating RBF model (static model) while the history of all scan-line signal data is tracked by means of an adaptive 1-D RBF model (adaptive model). The static model is re-computed for each new data as the best approximation to the data. The adaptive model is initialized once as the best approximation to the data and then updated for each new scan-line data by a small amount determined by the adaptation rate μ. For non-defective behaviour of the signal, the static approximation to the scan-line data is close to the adaptive approximation to the history of the scan-line data. Hence, the distance computed between the two models is small.

When a defective behaviour is encountered, the static approximation immediately reflects the defect behaviour while the adaptive approximation, because of its larger time constant, still reflects the regular non-defective behaviour. Hence, a large mismatch results between the two models, resulting in a large model-to-model distance metric.

(a) Determination of the Static Model Parameters

The model parameters which approximate the m[th] scan-line data are derived by minimizing the mean-squared-error (MSE) between the scan-line samples and the model approximation. The total approximation error over the m[th] scan-line data is given by the expression

$$E[m] = \sum_{n=1}^{N} \left(r_m[n] - \hat{r}_m[n]\right)^2. \tag{2}$$

To determine the parameter values minimizing the objective function in Eq.2, we take the partial derivatives with respect to the model parameters. When the approximating model is also substituted in the resulting equation, one obtains

$$\frac{\partial E[m]}{\partial p_i} = \sum_{n=1}^{N} 2\left(r_m[n] - \sum_{m=1}^{M} p_m \exp\left[\frac{-(n-\mu_m)^2}{2\sigma_m}\right]\right) \cdot \left(-\exp\left[\frac{-(n-\mu_i)^2}{2\sigma_i}\right]\right), \tag{3}$$

which, when equated to zero gives the linear system of equations given by

$$\sum_{l=1}^{L} p_l \left\{ \sum_{n=1}^{N} \exp\left[\frac{-(n-\mu_l)^2}{2\sigma_l}\right] \exp\left[\frac{-(n-\mu_i)^2}{2\sigma_i}\right]\right\} = \sum_{n=1}^{N} r_m[n] \exp\left[\frac{-(n-\mu_i)^2}{2\sigma_i}\right] \tag{4}$$

for i =1,2,...,L. This system can be expressed in matrix form. Denoting the inside summations by α_{il} members of an $L \times L$ square matrix **A**, the parameter vector by **p** and the right hand side coefficients as β_i members of a vector **b**, this set of L equations can be written as

$$\mathbf{A} \cdot \mathbf{p} = \mathbf{b}. \tag{5}$$

The values for the model parameters which are optimal in the MSE sense can then be obtained as

$$\mathbf{p} = \mathbf{A}^{-1} \cdot \mathbf{b}. \tag{6}$$

(b) Determination of the Adaptive Model Parameters

The parameters of the adaptive model are once initialized to be equal to the static model parameters at the beginning of the algorithm processing. However, for the remaining of the processing, they are updated using a variation of the steepest descent iterative optimization procedure. The procedure is based on the popular Least-Mean Squares (LMS) algorithm (Haykin 1996). The choice of the steepest-descent procedure is based on the fact that we do not require a fast adaptation but a gradual and smooth one. The additional adaptation speed contributed by a technique such as Recursive Least Squares (RLS) comes at a significant computational cost and is not justified for this application.

The speed of adaptation for the present procedure is governed by an adaptation rate parameter μ. Specifically, for each new scan-line signal data, the parameters of the adaptive model are updated along the direction of the steepest descent towards the optimum parameter values for the given data. This direction is determined by the negative gradient of the objective function with respect to the parameters. Hence the update equations for the adaptive RBF model parameters are given by

$$\mathbf{p}_{m+1} = \mathbf{p}_m - \mu \nabla E[m] \tag{7}$$

$$\mathbf{p}_{m+1} = \mathbf{p}_m - 2\mu\{\mathbf{A}_{m+1}\mathbf{p}_m - \mathbf{b}_{m+1}\} \tag{8}$$

where $\mathbf{A}_{m+1}$ and $\mathbf{b}_{m+1}$ are those determined from the current scan-line data.

(c) The Model Distance

Standard Euclidean distance is used as the model distance between the static and the adaptive model and is given by

$$\begin{aligned} |\mathbf{p}_s - \mathbf{p}_a|_2 &= \sqrt{(\mathbf{p}_s - \mathbf{p}_a)^T \cdot (\mathbf{p}_s - \mathbf{p}_a)} \\ &= \sqrt{\sum_{l=1}^{L} (p_{sl} - p_{al})^2} \end{aligned} \tag{9}$$

(d) Detection Threshold

The model distance computed for each scan-line data index m constitutes a model mismatch signal $d[m]$ which is subjected to a threshold based peak detection to determine the binary detection $D[m]$.

A fixed threshold can be used to perform the detection. However an adaptive threshold scheme is used in this study to improve the detection sensitivity when the background noise in the detection signal is low and to reduce false alarms when the detection signal is noisy.

The adaptive threshold works by keeping and updating two values, namely a partial mean level $\mu_d[m]$ and a partial variance level $\sigma^2[m]$. As long as no anomaly is detected, these levels are updated according to the equations

$$\mu_d[m+1] = \frac{\mu_d[m] \cdot m + d[m+1]}{m+1} \tag{10}$$

$$\sigma_d^2[m+1] = \frac{\sigma_d[m] \cdot m + (d[m+1] - \mu_d[m+1])^2}{m+1} \tag{11}$$

An anomaly is detected when the condition in Eq. 12 is satisfied. Here t_d is the threshold of detection. In this case, the adaptation of the mean and variance is not performed for the duration of the detection so as not to corrupt these parameters which reflect the normal behaviour of the image.

$$(d[m] - \mu_d[m])^2 > t_d \cdot \sigma_d^2[m] \tag{12}$$

(e) Post Processing of Detected Anomaly

The most important stage of the algorithm is the detection of the anomaly in the image to indicate the presence of a defect. However, once the defect is located, it also needs to be sized across the strip image and if possible, classified. This is achieved through a second stage of post-processing, in particular on the region indicated by the detection stage. Although the detection algorithm proposed can be easily applied to other application domains with similar strip material inspection needs, this post-processing stage is more application domain specific. Here a solution for a particular application domain will be considered.

As it is illustrated in the experimental results section, we consider in particular two types of defects from the application domain of grinded glass edge inspection. The first type of these defects are "shiner" defects and are composed of the lack of proper grinding at the middle of the glass edge. This type of defect appears dark to oblique illumination while the properly grinded region appears light due to the scattering of the incident illumination. The second type of defect we consider is called an "edge chip" and is the breaking of a small piece of glass from the region where the glass surface and grinded edge meet. This type of defect is usually harder to detect since the edge signal is particularly noisy on the sides and the chip appears as a small deviation in the edge thickness in this region.

To determine the type and across dimension of the defect the following procedure is applied. First, the average values of edge starting and edge ending values are extracted from before the beginning and after the ending of the defect region along the scanning direction. Then the defect region is uniformly sampled along the scanning direction. For each resulting scan-line segment, the signal background level is measured and a signal threshold is determined. The threshold is used to determine the edge location and number and locations of threshold crossings along the edge. For very small defect

lengths along the scanning direction, only a single sample from the centre may be considered for this sampling.

Any major deviation from the average edge starting and ending positions around the defect region is considered as a side defect (edge chip) with its side location information. The maximum value across the defect-sampling of any such deviation provides the across size of a side defect. Also, any additional threshold crossings inside the edge identify an inside defect (shiner). The size is measured as the maximum separation between the beginning-crossing and the ending-crossing across the defect-sampling.

Parameter Selection for the Application Domain

The following is a discussion of a reasonable set of guidelines for the selection of some algorithm parameters:

Scaling Factor

The signal may be pre-processed with a scaling and clipping before the detection stage is performed. For the present application domain, from the experimental data, it is observed that that a fixed scaling can be used throughout the detection stage. However, with varying camera/edge distance and dynamic illumination power control, an adaptive procedure may also be adopted.

Gaussian Functions

The number of the Gaussian functions used in the approximation determine how well the edge signal is approximated. Therefore, a larger number means a better approximation. However, the increasing number increases the computational complexity of the approximation and decreases the smoothing effect, resulting to also model the noise. This is clearly not desirable. Therefore, the choice should be as small as possible as long as a distance between the static and adaptive models has a significant enough peak in a defect region to allow detection. M=3 or M=5 Gaussian functions whose centers are distributed along the edge is observed to provide good results. We have preferred an odd number of Gaussian functions due to the symmetry of the signal and in order to have maximum sensitivity in the center of the image strip.

The Gaussian means are determined to provide a uniform distribution along the edge. For the M=3 case, one mean can be placed in the center of the edge and remaining two on the estimated edges. Small, gradual changes on the edge will not have a serious impact on the approximation.

The variances of the Gaussian functions are all the same and determined by the choice of their number and mean values. More specifically, the distance between two adjacent Gaussian functions determines this choice. The main criteria is to obtain a smooth enough approximation. A variance value of $\sigma = 2.5d$ where d is the distance between adjacent Gaussian functions gives an acceptable smoothness. This value is used for the approximations in Figure 1.

Adaptive Model Adaptation Rate

This value determines how fast the adaptive model will follow the changes in the edge signal. Too small a value will render the adaptive model fixed, which will not be able to track a gradual change in the edge signal. Too large a value will cause the adaptive model to follow the changes in the edge signal very closely and the model distance signal will always remain small making detection very difficult if not impossible. For a reasonably steady edge signal, values in the range 0.0005 to 0.005 are found to be reasonable choices for this application.

Detection Threshold

This threshold determines the sensitivity of detecting a defect and also affects the size measurement of the defect along the strip direction. As the threshold increases, only larger disturbances on the edge will trigger a detection. On the experimental samples considered for this application domain, a threshold value of 10 to 20 were appropriate choices. The parameter range can be tuned by experimentation with the application domain. This parameter is considered to be the only user controllable parameter to adjust the sensitivity of the overall system so as to eliminate the detection of very small defects.

4 EXPERIMENTAL RESULTS

For the experiments, we consider the application domain of grinded glass edge inspection. The edge is illuminated with coherent light at an oblique angle. The properly grinded edge is a scattering surface and back scatters enough light to generate a light signal. The grinding problems and missing parts on the edge can be visually observed to be present in the signal. Figure 4 illustrates the two aforementioned defect types on the grinded glass edge. Figure 5

presents the detection stage results for the more difficult case of an edge chip. The model mismatch signal is illustrated in the first part of the figure while the detection signal with the determined beginning and ending of the image anomaly is illustrated on the second part. From this figure, one can observe that the model mismatch based detection procedure successfully reduced the image event detection into a one dimensional peak detection task.

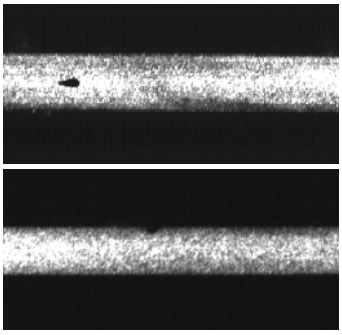

Figure 4: Examples of two important defect types from grinded glass edge inspection. (a) "Shiner" grinding problem (b) Edge chip (upper centre of the image).

Detection SNR with Signal Scaling

One interesting observation of the experimental results is the improvement of the detection performance of the algorithm with a software scaling of the image signal. In reality, the noise present in the signal is primarily due to the coherent nature of the illumination and the resulting effects. Although software scaling up of the image intensity may roughly correspond to an increase in physical illumination intensity, the noise is expected to scale with the signal and hence no SNR improvement is expected.

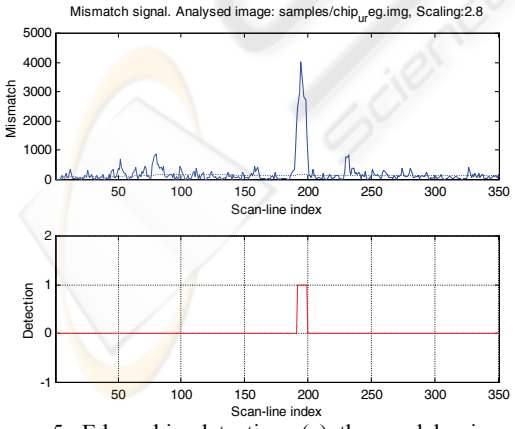

Figure 5: Edge chip detection. (a) the model mismatch signal, (b) the detection signal based on a user specified threshold.

However, it is observed that when the signal is scaled up so that higher intensity noise is clipped at the upper limit of the dynamic range of the signal, this has an overall positive effect on the performance of the model mismatch based detection. In fact, this positive effect is also visually apparent from the image data as can be seen in Figure 6.

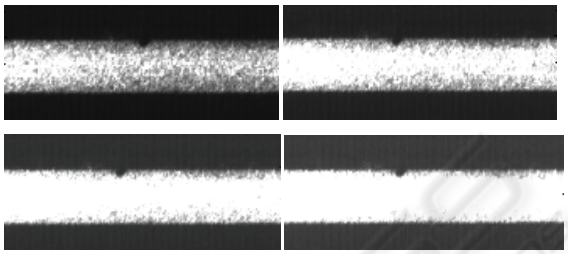

Figure 6: Edge chip defect images for software scaling of the image signal for scaling factors of *s*=1.0, 1.5, 2.0 and 2.5 respectively from top left to bottom right.

The model mismatch signal for the first case of s=1.0 and the last case of s=2.5 are illustrated in Figure 7 below. Assuming that the "signal" in the model mismatch signal is the defect peak and the background variation is the noise, one can conclude that the SNR relevant to the detection algorithm clearly improves. These results are also in agreement with a recent study (Sakurai et al., 2002) in the field of semiconductor inspection.

Experiments have been also conducted to assess the sensitivity of the detection algorithm for different defect sizes and positions on the image signal. For this purpose, a set of simulated defects have been generated with characteristics similar to the observed defects. The lack of a large selection of real defect samples have been a limiting factor at this point. The results for these experiments are summarized in the following sections.

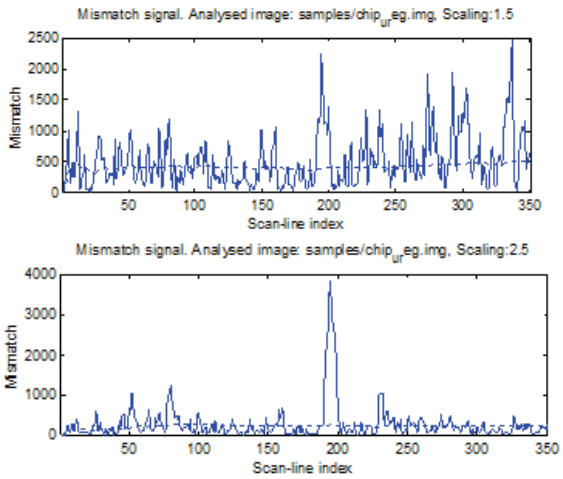

Figure 7: Illustration of model mismatch signal for the edge-chip defect for scaling factors *s*=1.5 and 2.5 respectively.

Detection Sensitivity with Defect Size

Figure 8 illustrates the set of simulated defects generated on the grinded glass edge signal with one real "shiner" defect sample (at the very right of the image data). The model mismatch signal is also illustrated in the figure and indicates the expected degrading of the performance with defect size. A total of 10 defects are considered on the glass edge (which is considered to be the more challenging case) with decreasing size from 1.3mm down to 0.1mm. The figure clearly illustrates the limit of detection which is at defect # 6 at 0.51mm.

The experiments with the defect location across the image data show a small amount of variation with the sensitivity remaining at a promising level. This is illustrated in Figure 9 for a simulated defect size of 0.91mm. Note that all defects including the ones on both sides (corresponding to edge chip defects) are detected for this defect size. The reason for the sensitivity variation illustrated is the presence of a mixture of Gaussians as the signal approximation tool with different Gaussian mean locations across the edge signal. The number of Gaussians have been set to M=5 for the experiment shown in the figure. A smaller M=3 value also leads to an operational system with less computational complexity but with a more severe sensitivity variation across the image.

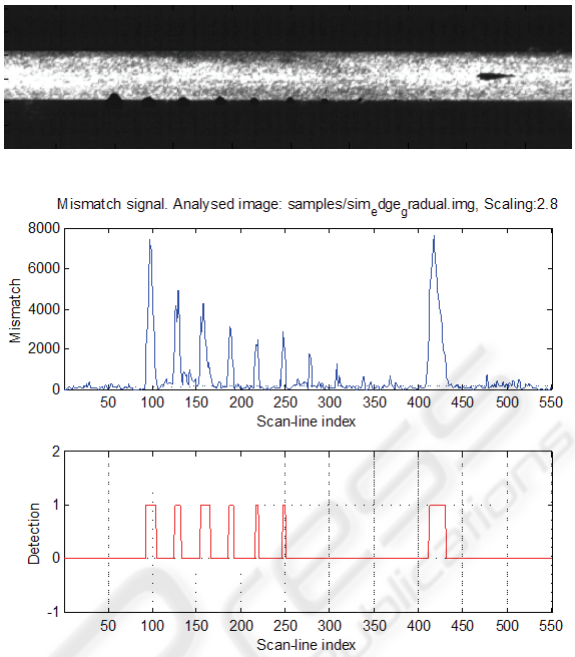

Figure 8: Experiment on detection performance with varying defect sizes. 10 simulated edge chips and a real "shiner" defect is present in the image.

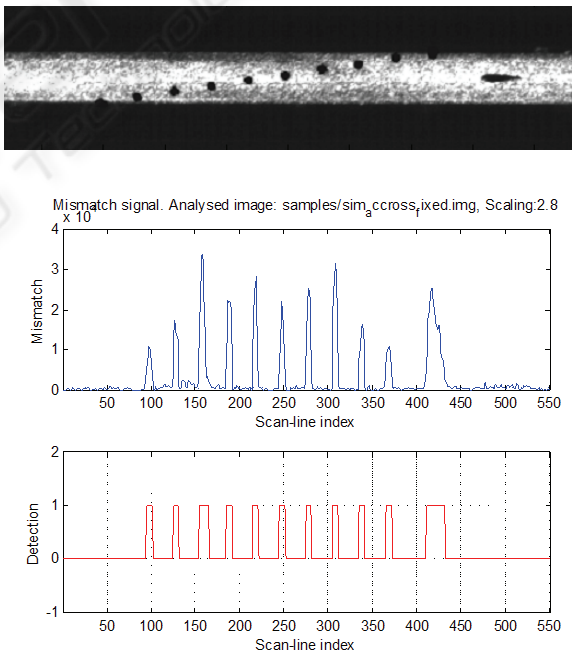

Figure 9: Experiment on algorithm sensitivity across the image. Simulated defect size is 0.91mm.

5 CONCLUSION

A model mismatch image event detection method based on a 1-D Radial Basis Function Network approximator for inspecting scan-line images of strip materials is presented. The method operates on the principle of detecting the mismatch between a static model derived from the scan-line and an adaptive model which tracks the slow changes in the signal. Thus the detector can accommodate slow variations in the image while keeping sensitive to the fast anomalies (defects). Experimental results on real defect samples and simulated defects have shown promising performance results in an application domain of grinded glass edge inspection.

REFERENCES

Ahmed W. et al., 1994. Adaptive RBF neural network in signal detection, *Proceedings of IEEE International Conference on Circuits and Systems*, pp. 265-268.

Alippi C. et al., 2000. Composite real-time image processing for railways track profile measurement, *IEEE Transactions on Instrumen-tation and Measurement,* Vol. 49, No. 3, pp.559-564.

Cho, C.; et al., Development of Real-Time Vision-Based Fabric Inspection System, *IEEE Transactions on Industrial Electronics,* 2005*,* Vol. *52*, No. 4., pp. 1073-1079.

Haykin. S. 1996. *Adaptive Filter Theory*. (3rd edition). NJ: Prentice Hall.

Haykin, S. 1999. *Neural Networks: A Comprehensive Foundation*. Upper Saddle River, NJ: Prentice Hall.

Kim, J.H. et al., 2001 A high speed high resolution system for the inspection of TFT LCD, *Proceedings IEEE Int. Symp. Industrial Electronics ISIE*, pp. 12–16

Leung H. et al., 2002. Detection of small objects in clutter using a GA-RBF neural network, *IEEE Transactions on Aerospace and Electronic Systems*, Vol. 38, No. 1, pp 98-118.

Malamas, E.N. et al., 2003 A survey on industrial vision systems, applications and tools *Image and Vision Computing, 21*, pp. 171-188

Poggio, T. and Girosi, F. 1990. Networks for approximation and learning. *Proceedings of the IEEE*, 78(9), pp. 1481-1497.

Sakurai, K. et al. 2002. Solution of Pattern Matching Inspection Problem for Grainy Metal Layers, *IEEE Transactions on Semiconductor Manufacturing,* Vol. 15, No. 1. pp 118-126.

Shen M. et al., 2005. Real-time detection of signals in noise using normalized RBF neural network, *Proceedings of IEEE International Workshop on VLSI Design and Video Technology*, pp. 165-168.